ACCSCIENCE PUBLISHING

International Journal of Bioprinting

RESEARCH ARTICLE

3D printing of the keloid scar using tunable GelMA-based bioinks for skin fibrosis modeling

Laurensia Danis Anggradita[1,2†], Murugaiyan Manimohan[3†], Sung Sik Hur[1†], Taekyun Kim[1,2], Wonjong Seon[1,2], Mohamed Aboobucker Sithique[3], Seung Min Nam[4*], and Yongsung Hwang[1,2*]

[1]Department of Integrated Biomedical Science, Soonchunhyang Institute of Medi-bio Science (SIMS), Soonchunhyang University, Cheonan, Chungnam 31151, Republic of Korea

[2]Department of Integrated Biomedical Science, Soonchunhyang University, Cheonan, Chungnam 31151, Republic of Korea

[3]PG & Research Department of Chemistry, Islamiah College, Thiruvalluvar University, Vaniyambadi, Tamil Nadu 635752, India.

[4]Department of Plastic and Reconstructive Surgery, Soonchunhyang University College of Medicine, Soonchunhyang University Bucheon Hospital, Bucheon, Gyeonggi 14584, Republic of Korea

(This article belongs to the *Special Issue: Intelligent 3D Bioprinting Strategies for Future Regenerative Medicine*)

Abstract

The development of mechanically tunable and cytocompatible hydrogels is critical for advancing three-dimensional (3D) bioprinting in tissue engineering. Here, we report a composite bioink composed of gelatin methacrylate (GelMA), methylcellulose, sodium alginate, and laponite-RDS. This formulation supports extrusion-based printing without ionic crosslinkers, mimics the extracellular matrix (ECM), and maintains stable viscoelasticity under physiological conditions (37°C, pH 7.4). Electrostatic and hydrogen bonding interactions among the charged polymers enhance pre-gel viscosity, shear-thinning behavior, and print fidelity. To evaluate its potential in disease modeling, patient-derived keloid fibroblasts were encapsulated in 3D-bioprinted constructs using two GelMA-based formulations with different stiffness levels, such as soft (G4A1M1R1, 2.1 kPa) and stiff (G5A1M1R1, 7.9 kPa), chosen to replicate the mechanical properties of normal dermis and keloid tissue, respectively. Both constructs exhibited excellent cell viability after three days, confirming cytocompatibility. Furthermore, matrix stiffness significantly regulated fibrotic gene expression. The stiffer hydrogel induced higher expression of *COL1*, *MMP2*, and *IL6*, suggesting enhanced myofibroblast activation and ECM remodeling. Immunofluorescence staining further confirmed elevated protein levels of α-SMA, FSP1, and actin stress fibers (F-actin) in the stiff construct, consistent with keloid pathology. Taken together, these results demonstrate that the GelMA-based bioink enables stiffness-dependent modulation of fibrotic responses, offering a simplified yet relevant 3D model of fibrotic skin. This platform may provide a useful basis for future studies on keloid progression and preliminary antifibrotic drug screening.

Keywords: Bioinks; Bioprinting; Keloid; Shape fidelity; Skin fibrosis; Viscoelastic properties

[†]These authors contributed equally to this work.

***Corresponding authors:**
Seung Min Nam (zodiac1003@schmc.ac.kr)

Yongsung Hwang (yshwang0428@sch.ac.kr)

Citation: Anggradita LD, Manimohan M, Hur SS, *et al.* 3D printing of the keloid scar using tunable GelMA-based bioinks for skin fibrosis modeling. *Int J Bioprint*. 2025;11(4):446-461. doi: 10.36922/IJB025160154

Received: April 19, 2025
1st revised: July 8, 2025
2nd revised: July 23, 2025
Accepted: July 23, 2025
Published Online: July 23, 2025

1. Introduction

Three-dimensional (3D) bioprinting has emerged as a transformative technology in tissue engineering and regenerative medicine, enabling the fabrication of artificial tissues and organ-like constructs that replicate native biological structure and function.[1,2] Among the various techniques, extrusion-based bioprinting allows for the precise deposition of cell-laden hydrogels within predesigned architectures to generate biomimetic platforms for tissue-specific applications.[3] Central to the success of this approach is the development of suitable bioinks—composite materials that integrate living cells with tunable biomaterials—to ensure high print fidelity, mechanical stability, and cytocompatibility throughout the printing and maturation processes.

A range of natural polymers and nanomaterials have been explored as bioink constituents, including gelatin methacrylate (GelMA), alginate, methylcellulose (MC), and laponite-RDS.[4,5] GelMA, a photo-crosslinkable gelatin derivative, is widely used for its cytocompatibility, cell-adhesive motifs, and tunable mechanical properties, which can be modulated by its concentration and the degree of methacrylation.[6–8] Alginate, a non-toxic polysaccharide, offers excellent printability through ion-induced gelation with divalent cations such as Ca^{2+}.[9] When blended with GelMA, it has been shown to enhance mechanical properties and improve matrix support for cell attachment.[10] However, excessive crosslinking or increased polymer density can hinder extrusion, prompting the need for rheological modulators.

MC serves as one such modifier. As a thermoresponsive polymer, MC enhances viscoelasticity and contributes to bioink cohesion by undergoing a sol–gel transition via hydrophobic interactions and reduced hydrogen bonding upon heating.[11–13] Its incorporation enables improved extrusion performance and structural fidelity at ambient temperatures. Laponite-RDS, a synthetic nanoclay, forms electrostatic interactions with charged polymers, thereby increasing viscosity, enhancing shear-thinning behavior, and modulating pore structure within the hydrogel matrix.[14] Beyond its physical reinforcement, laponite-RDS has demonstrated the ability to support a range of biological functions, including stem cell differentiation, migration, and neural regeneration, making it a promising additive in bioactive bioinks.[15–17]

Keloids are pathological fibrotic scars characterized by excessive collagen deposition, tissue stiffening, and abnormal extracellular matrix (ECM) remodeling. These lesions extend beyond the original wound site and are driven by aberrant fibroblast activation—primarily through TGF-β1 signaling—which leads to increased migratory activity, matrix production, and upregulation of fibrosis-related genes, including the members of MMP, LOX, and LOXL gene families.[18] The development of reliable *in vitro* models that recapitulate the keloid microenvironment is essential for understanding disease mechanisms and screening antifibrotic therapies. While several natural polymers such as collagen, gelatin, alginate, chitosan, and fibrin have been used to construct skin models,[19] the need remains for bioinks that are both biocompatible and mechanically tunable—particularly for modeling stiffness-sensitive fibrotic phenotypes.

Recent advances in 3D bioprinting have enabled the fabrication of stiffness-tunable artificial keloid constructs capable of supporting cell viability, mimicking keloid-like ECM architecture, and recapitulating relevant signaling pathways.[20] Building upon these advances, we developed a composite bioink system comprising GelMA, sodium alginate, MC, and laponite-RDS, designed to replicate the fibrotic microenvironment of keloid tissue through mechanical tuning and cell-instructive matrix design.

In this study, we systematically evaluated the contributions of each bioink component to matrix stiffness, viscosity, viscoelasticity, degradation behavior, and cell compatibility. Using patient-derived keloid fibroblasts encapsulated in these hydrogels, we established a 3D-bioprinted keloid model that supports cell viability and fibrosis-associated gene expression. This platform offers a robust and modular approach for engineering disease-specific skin models and lays the groundwork for future applications in personalized medicine and antifibrotic drug screening.

2. Materials and methods

2.1. Bioink preparation

GelMA was synthesized as previously reported.[21] Briefly, 10% (w/v) gelatin (cat# G1890, Sigma-Aldrich, St. Louis, USA) was dissolved in deionized water under continuous stirring at 60°C. Next, 8 mL of methacrylic anhydride (# 276685, Sigma-Aldrich, USA) was added dropwise while stirring. After 2 h of reaction, deionized water was added, which was maintained for another 30 min. Subsequently, the solution was dialyzed using a dialysis membrane (MWCO; approximately 12–14 kDa; Spectrum Laboratories, USA) at 55°C for 7 days. Following dialysis, the solution was filtered and lyophilized.

To prepare a bioink blend, lyophilized GelMA was dissolved in phosphate-buffered saline (PBS) and incubated at 60°C for 1 h to ensure proper GelMA dilution. Next, MC powder (cat# M7027-250G, Sigma-Aldrich, USA), alginate (cat# J61887-30, Alfa Aesar, USA), and laponite-RDS (cat# LAPONITE-RDS, BYK, Germany) were added

to the GelMA solution. To induce photocrosslinking of the bioink after printing, 0.5% (w/v) Irgacure 2959 (cat# 55047962; BASF, Germany) was added to the bioink blend. The final mixture was stirred at 25°C using a magnetic stirrer for 4 h at 120 rpm. This process yielded a composite bioink composed of GelMA (G), alginate (A), MC (M), and laponite-RDS (R), referred to as G*x*A*x*M*x*R*x*. The "*x*" determines the concentration (w/v) as described in Table S1.

2.2. Rheology testing of uncrosslinked hydrogel

The viscosity and viscoelasticity of the uncrosslinked bioinks were determined using a Kinexus rheometer (Kinexus Ultra+, Malvern Panalytical, England). First, the pre-gel of the bioink was loaded onto the rheometer plate, and the gap between the upper geometry and the plate was set to 0.5 mm. The sample was equilibrated to 37°C before testing. Viscosity was measured using a cone-plate geometry, with shear rates ranged from 0.1 to 2 s^{-1} across a logarithmic scale with 20 intervals. Viscoelasticity was determined by amplitude and frequency sweeps using a parallel-plate cone. For the amplitude sweep, the applied shear strain ranged from 0.01 to 5%, at a constant oscillation frequency of 1 Hz, with a sampling density of 20 points per logarithmic decade. The frequency sweep was measured from 0.01 to 50 Hz at a constant strain of 2%.

2.3. Mechanical testing of crosslinked hydrogel

Mechanical properties were measured using an Instron device (EZ-SX; SHIMADZU, Japan) in compressive mode. Digital calipers were used to measure the diameters and heights of the hydrogels. Compression was applied from 0 to 70% strain at a rate of 1 mm/min at room temperature. Data were recorded when the ramp head contacted the hydrogel and registered a force of 0.01 N. Testing was terminated when the hydrogel broke. To calculate the Young's modulus (E), we used the linear region of the stress–strain curve with 10% strain. For each formulation, the average Young's modulus was calculated from three replicates. Data analysis was performed using MATLAB (MathWorks, USA). A two-degree polynomial interpolation was used to determine the Young's moduli at intermediate concentrations. Table S1 lists Young's moduli measured at different concentrations. The Young's moduli for each group are summarized in Figure S1. Table S4 summarizes the mechanical properties of each group, including toughness, stress, and strain at break.

2.4. Shape fidelity

The hydrogels were printed using the Inkredible+ Bioprinter (CellInk, Göteborg, Sweden) at room temperature. A square grid pattern (13.5 × 13.5 mm with 3 × 3 = 9 pores) was printed on Petri dish. For printing, 2 mL of bioink solution was added to the cartridge. Printing was performed using 22G blunt conical bioprinting nozzles (ID: 410 μm). The applied pressure ranged from 3 to 6 kPa, depending on the bioink formulation, as described in Table S2. The printing process was performed at a feed rate of 1500 mm/min and a layer height of 0.8 mm. After printing, the hydrogels were polymerized under ultraviolet (UV) light (365 nm; Blak-Ray XX-15L; UVP, Upland, USA) for 5 min. The hydrogels were then equilibrated in PBS for 24 h. Shape fidelity was assessed by comparing the measured pore size with the designed pore size using the following formula[22]:

$$\text{Shape fidelity} = \left(\frac{a \times b}{a' \times b'} \right) \times 100\% \quad \text{(I)}$$

where a and b are the designed dimensions of the pore base, and a' and b' are the corresponding dimensions of the actually printed pore base.

Detailed information on the calculation of shape fidelity is provided in Figure S2 and Table S6.

2.5. *In situ* hydrogel

Patient-derived keloid tissue was obtained from the Soonchunhyang University of Bucheon Hospital, according to the protocols approved by the Institutional Review Board of Soonchunhang University Bucheon Hospital (SCHBC_IRB_2017-08-010). This study was conducted in accordance with the 1964 Declaration of Helsinki and its subsequent amendments. The dermal layer was separated, and keloid dermal fibroblasts were isolated following a previous protocol.[18] The cells were cultured in Dulbecco's modified Eagle's medium (10-013-CV, Corning, USA) supplemented with 10% fetal bovine serum (cat# 35-015-CV, Corning, USA), 1% l-glutamine (200 mM; cat# 25030081, Gibco-BRL, USA), and 1% penicillin–streptomycin (15140122, Life Technologies, USA). The bioinks were prepared in PBS at 80% of the total volume. Next, the cell pellet was resuspended in PBS at 10% of the total hydrogel volume and added to the bioink blend. For hydrogel encapsulation, cells were suspended at a density of 1 × 10^6 cells/mL for real-time polymerase chain reaction (qPCR) analysis and at 2 × 10^6 cells/mL for immunofluorescence staining and live/dead assays to enhance signal detection and cell representation. The solution was stirred for 15 min. This formed a cell-laden hydrogel with a total dissolved volume of 90%. Considering the 10% volume loss during hydrogel blending, we dissolved the *in situ* hydrogel in 90% of the total volume of PBS to prevent further dilution upon cell addition. The hydrogel was printed as a grid-like structure and subsequently exposed to UV light (365 nm; Blak-

Ray XX-15L; UVP, USA) for 5 min for crosslinking. The hydrogel was kept in the growth medium for 3 days before further experiments.

2.6. Live/dead cell viability assay

Cell viability was assessed three days after the printing process using the Live/Dead Viability/Cytotoxicity Kit (cat# 3 L-3224, Invitrogen, USA), following the manufacturer's instructions. After staining, the hydrogel was washed with PBS and imaged using a THUNDER Imager (Leica Microsystem, Germany) with 5× objective lens (N Plan; NA, 0.12; Cat# 11506303, Leica Microsystem, Germany) and an EVOS M700 imaging system (Thermo Fisher Scientific, Waltham, USA) equipped with a 10× water immersion objective lens (Fluorite; NA, 0.30), utilizing a stitching function to generate complete images of the hydrogel.

2.7. Real-time polymerase chain reaction

Total RNA was isolated from the hydrogel using TRIzol reagent (Cat# 15596018, Ambion, USA), and cDNA synthesis was performed using ReverTra Ace qPCR RT Master Mix with gDNA Remover (Cat# KMM-101, TOYOBO, Japan), following the manufacturer's instructions. Subsequently, qPCR was performed using a QuantStudio 1 Real-Time PCR System (Applied Biosystems, Foster City, USA) and SYBR Green Real-time PCR Master Mix (Cat# 4472918, TOYOBO, Japan). Table S3 lists the primers used for the qPCR. All experiments were performed in triplicate for each group. Glyceraldehyde 3-phosphate dehydrogenase (*GAPDH*) served as a housekeeping gene. The ΔC_t values were determined as $Ct^{target} - Ct^{GAPDH}$, and relative fold changes were calculated using the $2^{-\Delta\Delta Ct}$ method.[23]

2.8. Immunofluorescence

In situ hydrogels were fixed in 4% paraformaldehyde (PFA, Cat# CNP015-0500, CellNest, Korea) for 30 min and permeabilized with 0.3% Triton X-100 (Cat# TRX777.500, Bioshop, Canada) solution for 30 min at room temperature. Subsequently, hydrogels were blocked in a solution of 5% BSA for 30 min at room temperature. Hydrogels were then incubated in primary antibodies for 48 h at 4°C, followed by secondary antibodies for 24h at 4°C. Antibodies are listed in Table S4. Confocal imaging was performed using an LSM 710 microscope (Carl Zeiss, Germany) at the Soonchunhyang Biomedical Research Core Facility of Korea Basic Science Institute with a 10× objective lens (Plan-Apochromat; NA, 0.45; Cat# 420640-9900-000, Carl Zeiss, Germany). Tiled images were acquired using a THUNDER Imager (Leica Microsystem, Germany) with a 5× objective lens (N Plan; NA, 0.12; Cat# 11506303, Leica Microsystem, Germany).

2.9. Statistical analysis

Data were analyzed using GraphPad Prism version 10.3 (GraphPad Software, Inc., USA). Bar graphs represent mean values, with error bars indicating standard deviations. The statistical significance between two groups was assessed using Student's *t*-test, while comparisons among multiple groups were conducted using one-way analysis of variance followed by Tukey's post hoc test. Statistical significance was set at $^{*}p < 0.05$, $^{**}p < 0.01$, and $^{***}p < 0.001$.

3. Results and discussion

3.1. GelMA concentration as a biocompatible crosslinker

The G*x*A*x*M*x*R*x* bioink system was formulated through polyelectrolyte complexation and covalent crosslinking among GelMA (G), alginate (A), MC (M), and laponite-RDS (R), as illustrated in Figure 1. The variable "*x*" denotes the respective concentrations used (Table S1). Each component serves a distinct role: GelMA acts as a biocompatible crosslinker offering structural integrity and cell-adhesive moieties, while alginate, MC, and laponite-RDS modulate viscoelasticity and printability.

GelMA is an ampholytic polymer carrying both negative and positive charges. At acidic pH values below its isoelectric point, its amine groups are protonated, rendering it positively charged and enabling electrostatic interactions with the negatively charged MC to form polyelectrolyte complexes.[24] Concurrently, alginate contributes to the polymer network through nucleophilic attack by its carboxylic acid groups on the hydroxyl functionalities of MC, leading to ring-opening of the pyranose structure and formation of aldehyde intermediates.[25] These intermediates react with GelMA's amine groups, generating nitrogen-containing intermediate rings. Additionally, primary amines on GelMA can form stable amide bonds with carboxylic or ester groups on alginate, enhancing both intra- and inter-molecular crosslinking and improving hydrogel stability.[26] Furthermore, alginate and MC primarily interact with GelMA through physical entanglement and hydrogen bonding, which increase viscosity and enhance viscoelasticity. These interactions also promote shear-thinning behavior, thereby improving the printability of the hydrogel system.[27]

Laponite-RDS, a synthetic nanoclay composed of disc-like platelets (~15 nm diameter, ~1 nm thickness), features alternating trioctahedral and tetrahedral layers with interspersed magnesium and lithium ions surrounded by negatively charged silicate surfaces. This high charge density and surface area render it suitable for biomedical applications. In bioink formulations, laponite-RDS enhances mechanical stiffness, shear-thinning behavior,

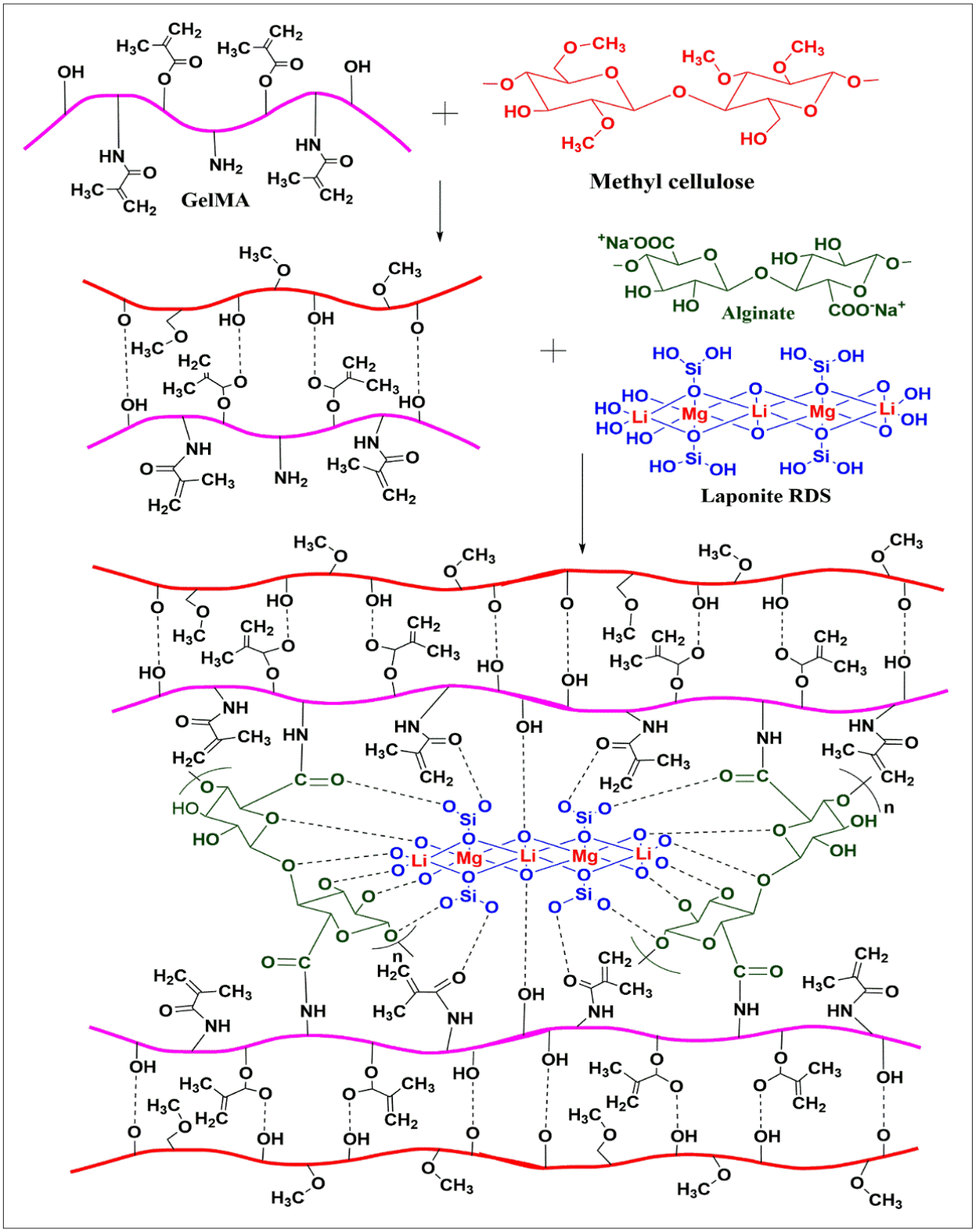

Figure 1. Preparation of gelatin methacrylate (GelMA), methylcellulose (M), alginate (A), and laponite-RDS (R) blended bioink (GxMxAxRx).

and surface roughness through interparticle interactions and water intercalation.[28] Its negatively charged surfaces can form ionic interactions with the positively charged amine groups of GelMA, thereby improving network stability and mechanical reinforcement.[29]

To investigate GelMA's role as a mechanical crosslinker, we compared bioinks with 4% (G4A1M1R1) and 5% (G5A1M1R1) GelMA content, representing soft and stiff hydrogels, respectively (Figure 2A). Despite the 25% increase in GelMA concentration, no statistically significant differences in viscosity or viscoelastic moduli were observed between the groups (Figure 2B–G). Both exhibited typical non-Newtonian, shear-thinning behavior, with viscosity decreasing as shear rate increased (Figure 2B–C). This property supports extrusion-based bioprinting, where low viscosity under shear facilitates flow and high viscosity post-extrusion maintains structural fidelity.[30] Frequency sweep analysis indicated stable viscoelastic behavior across both groups (Figure 2D, G), but compression testing revealed significantly higher stiffness in G5A1M1R1, with a Young's modulus of 7.9 ± 1.3 kPa compared to 2.1 ± 0.92 kPa in G4A1M1R1 (Figure 2H–I). These findings suggest that mechanical reinforcement primarily arises from enhanced GelMA crosslinking, rather than bulk rheological differences. Since GelMA relies on chemical crosslinking via photopolymerization rather than ionic or physical interactions, the resulting hydrogel remains stable under physiological ionic conditions, which might otherwise affect electrostatic interactions and compromise structural integrity (Figure 2J–K). Furthermore, slower degradation was observed in G5A1M1R1 (Figure S1C), indicative of a denser and more stable polymer network. Enhanced mechanical resilience and matrix stability are likely due to the increased density of covalent and non-covalent crosslinks formed at higher GelMA concentrations.[24,31] In summary, increasing GelMA concentration improves the mechanical performance, degradation resistance, and printability of the hydrogel, which are essential for supporting cellular viability and long-term culture in

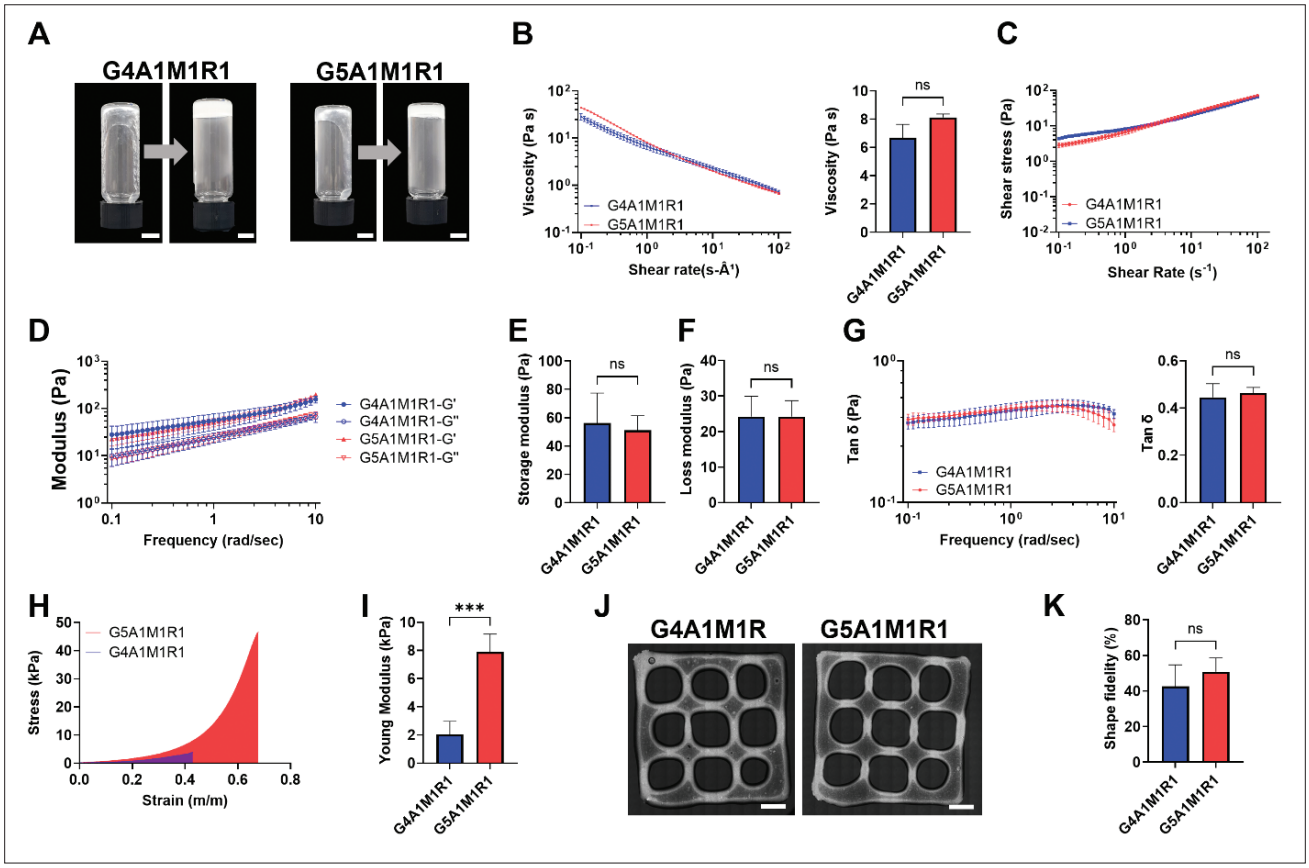

Figure 2. Effect of GelMA as a crosslinker on the rheological and mechanical properties of bioink. (A) Crosslinked hydrogel blend consists of GelMA (4 and 5% w/v), alginate (1% w/v), methylcellulose (MC) (1% w/v), and laponite-RDS (1% w/v). Scale bar: 5 mm. (B) Viscosity and (C–G) rheological properties of hydrogel blends with varying concentrations of GelMA. (H–I) Higher mechanical properties observed with higher crosslinker concentration. $^{*}p < 0.05$, $^{***}p < 0.001$. (J–K) Printability and structural shape fidelity of a hydrogel blend. Scale bar: 2.5 mm.

3D-bioprinted constructs. Although higher GelMA content can hinder extrusion due to nozzle clogging, this limitation can be overcome by co-formulating with alginate, MC, and laponite-RDS to preserve flow characteristics while maintaining structural fidelity.

3.2. Alginate as an elasticity enhancer

In extrusion-based bioprinting, viscosity and shear-thinning behavior are critical for achieving high-resolution structures while maintaining mechanical stability during and after deposition. Building on previous studies, we investigated the role of alginate as a viscoelasticity enhancer by comparing formulations containing different alginate concentrations: 0.5% (G5A0.5M1R1) and 1% (G5A1M1R1), without the use of multivalent cation crosslinkers (Figure 3A). As expected, the bioink with higher alginate concentration exhibited a substantial increase in viscosity (~76%) and more pronounced shear-thinning behavior (Figure 3B–C). This increase in viscosity reflects alginate's concentration-dependent chain entanglement, which improves printability by supporting controlled extrusion and better shape retention. Higher viscosity also enables faster structural recovery post-printing, a key parameter for high-fidelity bioprinting.

Both formulations displayed solid-like viscoelastic characteristics, with storage modulus (G′) consistently exceeding loss modulus (G″) over increasing frequencies (Figure 3D). Notably, the G′ of the 1% alginate group (G5A1M1R1: 50.17 ± 8.59 Pa) was more than twice that of the 0.5% group (G5A0.5M1R1: 19.50 ± 12.52 Pa), suggesting a significant enhancement in network stiffness (Figure 3D–E). This finding supports the role of alginate as a structural modifier that promotes stronger elastic responses within the composite hydrogel. Although the increase in G″ was not statistically significant (Figure 3F), it followed a similar upward trend.

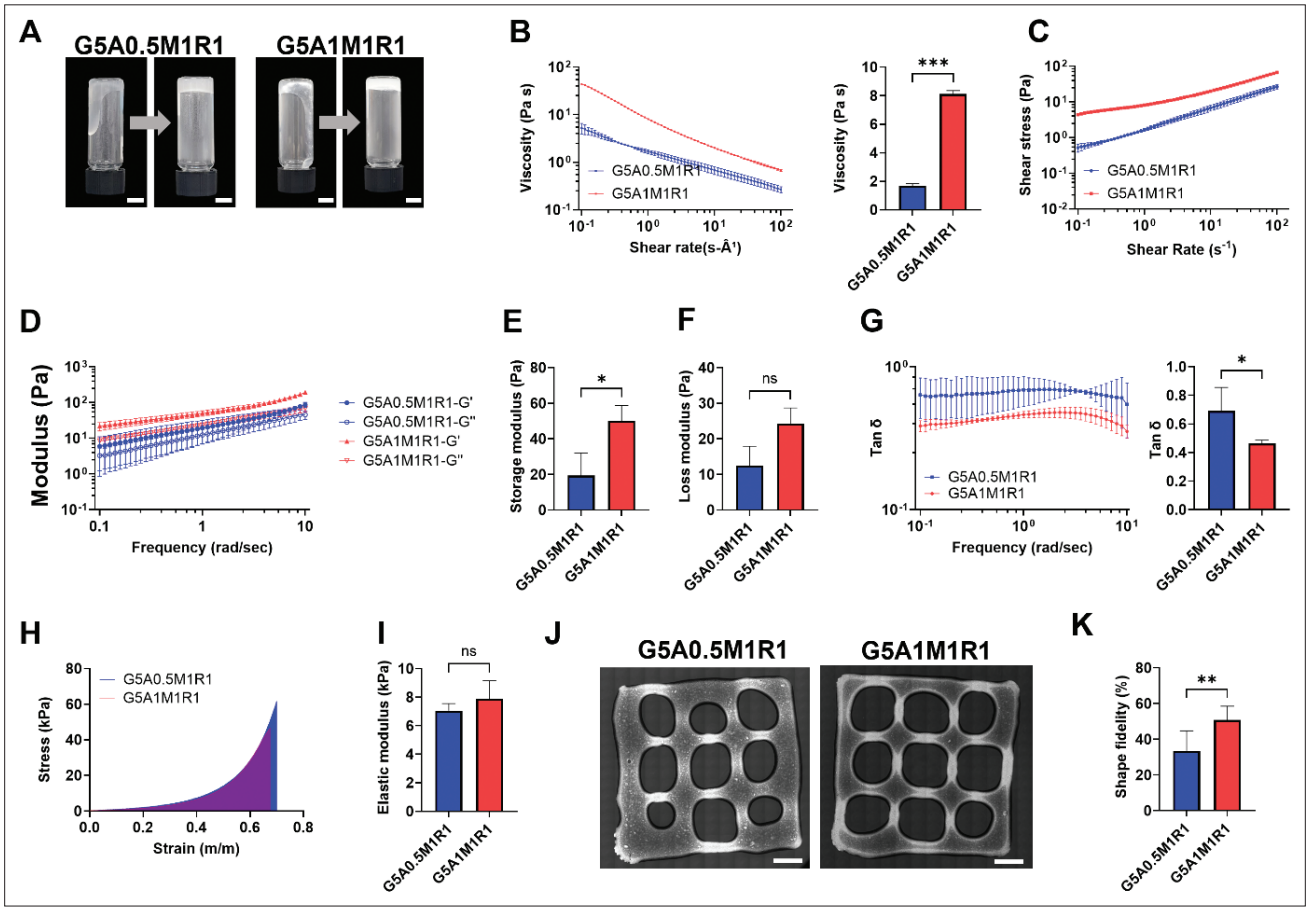

Figure 3. Role of alginate as a viscoelasticity enhancer. (A) Crosslinked hydrogel blend consists of GelMA (5% w/v), alginate (0.5 and 1% w/v), MC (1% w/v), and laponite-RDS (1% w/v). Scale bar: 5 mm. (B) Viscosity and (C–G) rheological properties of hydrogel blends with varying alginate concentrations. (H–I) Mechanical properties with varying concentration of alginate. *$p < 0.05$, **$p < 0.01$, ***$p < 0.001$. (J–K) Printability and shape structural fidelity of a hydrogel blend. Scale bar: 2.5 mm.

The damping factor (tan δ), defined as G″/G′, decreased in the G5A1M1R1 group (Figure 3G), indicating reduced viscous dissipation and a more dominant elastic component. This aligns with previous studies suggesting that gelatin–alginate hydrogels with tan δ values between 0.25 and 0.45 yield optimal print fidelity.[32] Interestingly, mechanical testing revealed slightly higher toughness in the lower alginate concentration group (Figure 3H, Table S5). This may be attributed to more efficient integration of alginate into the polymer matrix at lower concentrations, enhancing the load distribution within the hydrogel network. Although the difference in Young's modulus between groups was not statistically significant (Figure 3I), a slight increase was observed with higher alginate content, consistent with steric hindrance and chain entanglement effects.

In the absence of ionic crosslinkers, alginate's influence appears to arise primarily from physical entanglement with GelMA and MC chains, rather than stable ionic or covalent interactions. This physical contribution nonetheless improved the structural fidelity and reduced the degradation rate of the hydrogel, likely by shielding gelatin cleavage sites from enzymatic degradation (Figure S1C). Bioprinting trials demonstrated that incorporating 1% alginate, along with GelMA, MC, and laponite-RDS, enabled the formation of robust, well-defined structures at 25°C (Figure 3J), producing better printability properties (Figure 3K). These results confirm that alginate serves as an effective viscosity and elasticity enhancer, contributing to the mechanical performance, printability, and biological utility of the G*x*A*x*M*x*R*x* bioink formulation.

3.3. Enhancing viscosity by methylcellulose

One of the key limitations in extrusion-based bioprinting is the need to balance high-resolution printing with minimal shear-induced cellular damage. MC, a hydrophilic cellulose derivative, is widely used to increase viscosity and improve print fidelity while supporting cell viability. To evaluate the role of MC in our bioink system, we compared two concentrations—0.5% (G5A1M0.5R1) and 1% (G5A1M1R1)—while maintaining constant concentrations of GelMA, alginate, and laponite-RDS (Figure 4A).

Although increasing the MC concentration led to a 33% increase in viscosity, this enhancement was modest compared to that observed with alginate (Figure 4B). Both formulations retained a clear shear-thinning profile, which is critical for facilitating bioink flow during extrusion and maintaining structural integrity post-deposition.

Rheological analysis demonstrated improved viscoelasticity in the higher MC concentration group, though the changes were not statistically significant (Figure 4C–G). The increase in G′ and G″ suggests that MC modulates the hydrogel's mechanical response under deformation. Unlike previous reports that have described a Newtonian plateau at low to intermediate shear rates in MC-only solutions,[33] our composite formulation exhibited continuous shear-thinning behavior across all shear rates. This likely results from the combined effects of GelMA, alginate, and laponite-RDS, which modify the microstructural dynamics of the hydrogel network.

The 1% MC formulation also demonstrated enhanced mechanical integrity, as shown by a steeper stress–strain curve (Figure 4H) and improved toughness (Table S5). Moreover, the elastic modulus increased from 5.53 ± 1.03 kPa (G5A1M0.5R1) to 7.91 ± 1.26 kPa (G5A1M1R1), a 1.4-fold enhancement (Figure 4I). These improvements reflect the role of MC in reinforcing the hydrogel network and increasing resistance to deformation. In addition, the degradation rate was slower in the higher MC group (Figure S1C), which is consistent with MC-induced steric hindrance that reduces enzymatic accessibility to cleavage sites.

However, increased MC concentration could reduce the printability (Figure 4K) as the MC controlled shape fidelity and reduced spreading observed in the 1% MC group (Figure 4J). The combination of MC with alginate and GelMA allows for controlled deposition of even low-viscosity formulations by modulating the composite's viscoelastic response. Furthermore, MC is known to alter the hydrogel's microstructure and act as a rheological modifier, thereby slowing release rates and improving long-term stability.[34] Overall, increasing MC concentration enhanced viscosity, mechanical stiffness, and structural integrity, without compromising biocompatibility. The addition of MC also increased the loss modulus and yield stress of the hydrogel blend,[35] contributing to the robustness of printed constructs—especially when fine structural features and cell protection during printing are required.

3.4. Laponite-RDS controls rheological properties

Rapid degradation of hydrogels remains a key limitation for long-term applications in tissue engineering. To address this, laponite-RDS—a synthetic, discotic nanoclay—was incorporated into the bioink formulation to enhance rheological and mechanical properties. Laponite-RDS consists of alternating silicate layers with embedded magnesium and lithium ions, forming a charged, plate-like structure (~15 nm in diameter, ~1 nm in thickness) that imparts thixotropic behavior and high surface reactivity.[36]

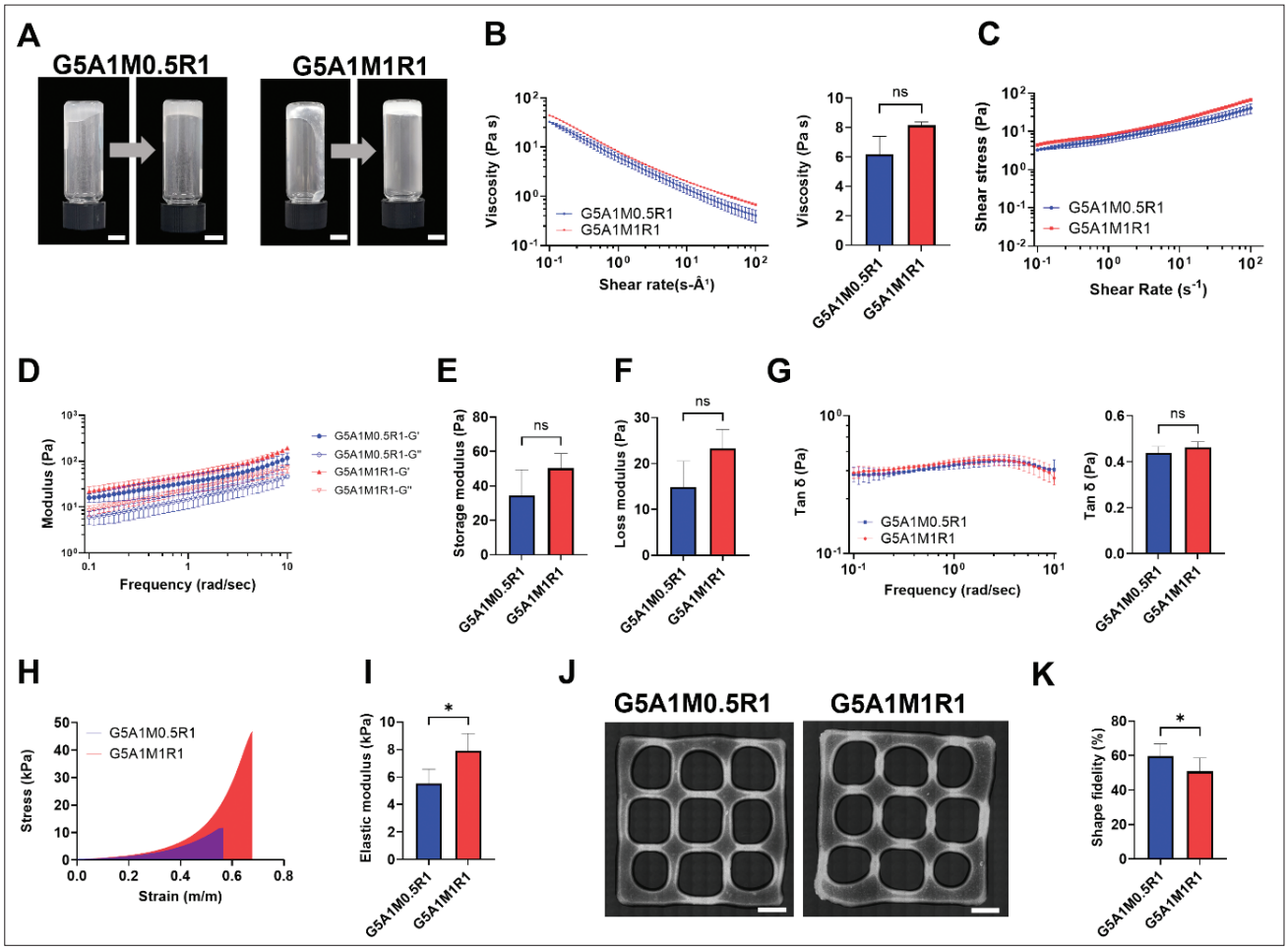

Figure 4. Tuning the viscoelasticity by increasing MC concentration. (A) Crosslinked hydrogel blend consists of GelMA (5% w/v), alginate (1% w/v), MC (0.5 and 1% w/v), and laponite-RDS (1% w/v). Scale bar: 5 mm. (B) Viscosity and (C–G) viscoelastic properties of hydrogel blends with varying concentrations of MC. (H–I) Increased viscoelasticity with a higher concentration of MC content. *$p < 0.05$. (J–K) Printability and structural shape fidelity of a hydrogel blend. Scale bar: 2.5 mm.

To evaluate its contribution, we compared formulations with (G5A1M1R1) and without (G5A1M1) laponite-RDS (Figure 5A). The inclusion of laponite-RDS increased viscosity by approximately 75%, contributing to the formation of a thicker and more cohesive bioink (Figure 5B). Both groups exhibited clear shear-thinning behavior, but the addition of laponite-RDS enhanced this effect, facilitating improved extrusion performance during printing.

Rheological profiling showed increased storage (G′) and loss (G″) moduli in the presence of laponite-RDS, with 62 and 47% increases, respectively (Figure 5C–G). Although the enhancement in elastic behavior was modest, the overall viscoelastic balance shifted toward greater rigidity. These effects are attributed to electrostatic interactions between the cationic amine groups of GelMA and the negatively charged silicate surfaces of laponite-RDS.[29] The disc-shaped laponite particles possess a net negative charge on their faces due to exposed silicate (SiO_4^{4-}) groups, while their edges carry a slight positive charge from divalent cations such as Mg^{2+} and monovalent Li^+. These charge distributions enable reversible ionic interactions with the amphoteric side chains of GelMA, contributing to increased pre-gel viscosity and enhanced network stabilization prior to photopolymerization. Interestingly, while the impact of laponite-RDS on G′ and G″ was consistent, the differences did not reach statistical significance (Figure 5G), suggesting that its primary function may be to fine-tune rather than drastically alter bulk viscoelasticity. Nevertheless, mechanical testing revealed a lower stress response and reduced toughness in the absence of laponite-RDS (Figure 5H, Table S5), indicating compromised structural integrity. The degradation rate was also higher in laponite-RDS-free

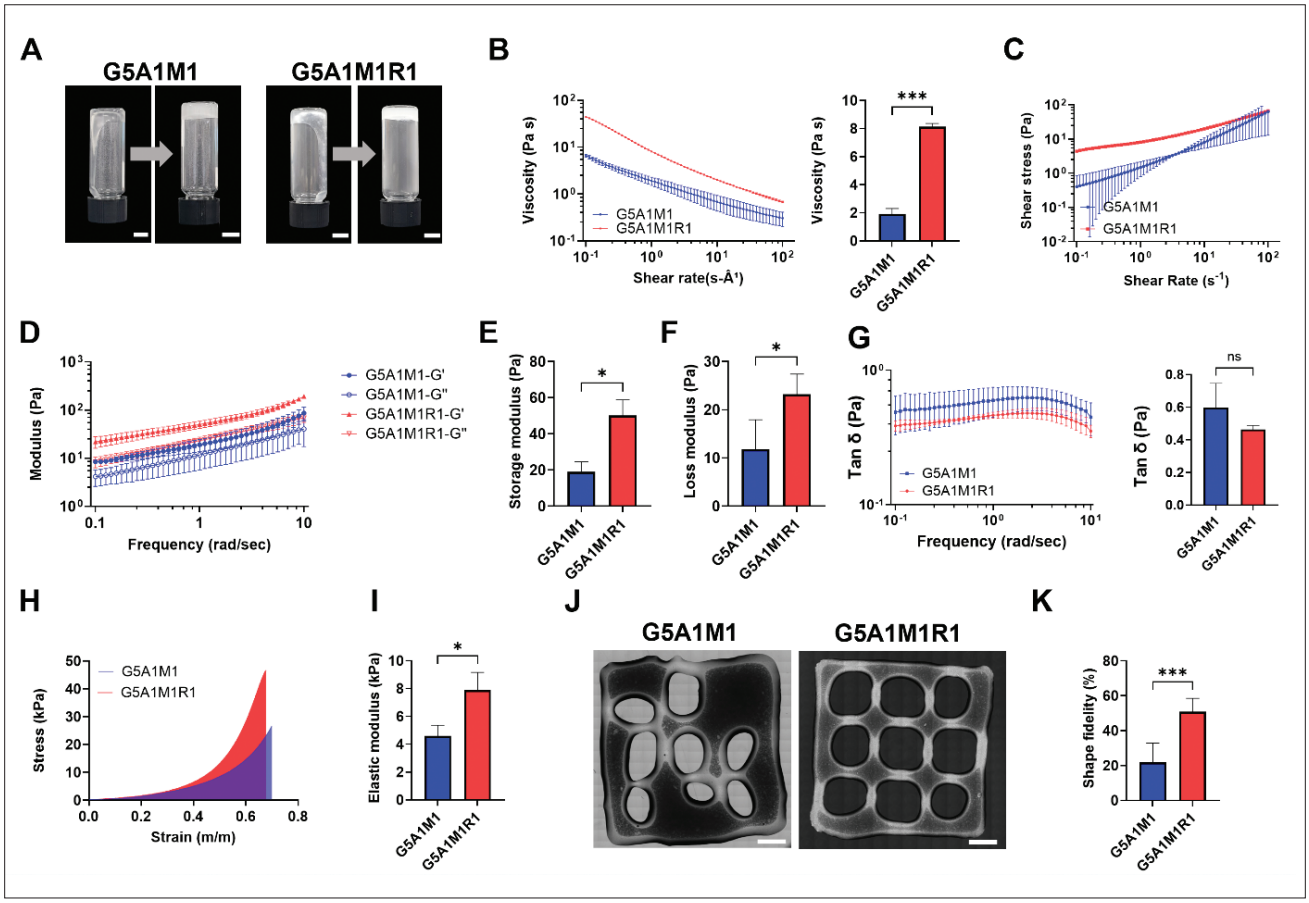

Figure 5. Incorporation of laponite-RDS enhances printability of bioink. (A) Crosslinked hydrogel blend consists of GelMA (5% w/v), alginate (1% w/v), MC (1% w/v), and laponite-RDS (0 and 1% w/v). Scale bar: 5 mm. (B) Viscosity and (C–G) rheological properties of hydrogel blends with and without laponite-RDS. (H–I) Laponite-RDS increases mechanical properties and (J–K) the structural shape fidelity of the hydrogel blend as a bioink. *$p < 0.05$, ***$p < 0.001$. Scale bar: 2.5 mm.

bioinks (Figure S1C), supporting the role of laponite in stabilizing the hydrogel network.

Laponite's contribution to mechanical reinforcement is further supported by Young's modulus measurements, which increased from 4.59 ± 0.79 kPa in the laponite-free group (G5A1M1) to 7.91 ± 1.26 kPa in the laponite-containing group (G5A1M1R1) (Figure 5I). These findings confirm that laponite-RDS enhances the elastic modulus, likely through increased crosslinking density and network entanglement.[37] Finally, printing performance analysis showed that laponite-RDS improved print fidelity by minimizing spreading and maintaining the printed geometry post-extrusion (Figure 5J–K). This improvement is attributed to physical crosslinking effects that influence key mechanical and rheological properties—including elastic modulus, swelling behavior, viscosity, and flowability—through electrostatic interactions, hydrogen bonding, hydrophobic interactions, and van der Waals forces. The locally charged polymers in the bioink—GelMA, MC, and alginate—can also interact with charged biomolecules such as antifibrotic drugs, potentially modulating cell behavior depending on the net surface charge.[38,39] Similarly, alginate (rich in COO– groups) and carboxymethylated MC interact with GelMA via hydrogen bonding and ionic entanglement involving amine and hydroxyl side chains.[35,40] While weaker than covalent crosslinking, these interactions contribute to shear-thinning behavior, increased yield stress, and enhanced pre-gel viscosity.

Upon UV-induced photopolymerization of GelMA, covalent crosslinks become the dominant contributors to the hydrogel's structural integrity. Nevertheless, pre-existing physical interactions such as hydrogen bonding, electrostatic entanglement, and polymer chain entanglement among GelMA, alginate, and MC remain important for modulating the viscoelastic behavior,

particularly under physiological conditions (pH 7.4, 37°C).[27,41,42] The hydrogel system exhibits rapid gelation, high yield stress, and prolonged stress relaxation, enabling efficient transitions between flow and solid states. These properties contribute to reliable extrusion, improved print fidelity, and stable construct formation during 3D bioprinting.

Collectively, these multiscale interactions, including ionic bonding, hydrogen bonding, and polymer network entanglement, synergistically regulate the rheological performance of the bioink. This cooperative behavior enhances the pre-print stability and post-print mechanical integrity, enabling the formation of cell-laden constructs with clinically relevant stiffness. Prior studies involving GelMA–clay–alginate systems have demonstrated similar synergistic effects,[43-45] supporting the design rationale and functional benefits of our composite formulation.

3.5. Biocompatibility of G*x*A*x*M*x*R*x* as a keloid skin model

Keloids are fibrotic skin disorders characterized by excessive ECM deposition, particularly collagen types I, and abnormal fibroblast behavior, leading to stiff, nodular lesions that extend beyond the original wound. A hallmark of keloid pathology is the activation of dermal fibroblasts into myofibroblasts, marked by elevated expression of fibrosis-related proteins such as α-SMA and FSP-1.[18,46] To model this pathophysiology *in vitro*, we encapsulated patient-derived keloid dermal fibroblasts within two GelMA-based bioink formulations: G4A1M1R1 (soft) and G5A1M1R1 (stiff). These compositions represented the lowest and highest stiffness values among all tested hydrogels (Figure S1A), enabling us to assess the impact of matrix stiffness on keloid fibroblast behavior. Importantly, the concentrations of MC, alginate, and laponite-RDS were held constant across both groups to minimize compositional variability and isolate stiffness as the primary variable. The selected formulations were specifically chosen to closely match the microscale elastic moduli of normal dermis (~2.4 ± 1.0 kPa) and keloid tissue (~14.2 ± 1.0 kPa), as previously reported.[47] Thus, this design allowed us to mimic physiologically relevant mechanical cues and assess mechanotransduction in a 3D-printed skin fibrosis model.

Live/dead assays performed 3 days post-encapsulation showed strong calcein-AM fluorescence, confirming high cell survival within the 3D-printed constructs (Figure 6A). These findings demonstrate the low cytotoxicity and excellent biocompatibility of the G*x*A*x*M*x*R*x* hydrogel system. Notably, key functional motifs such as RGD sequences and MMP-sensitive linkages are preserved during GelMA photopolymerization, facilitating cell adhesion and matrix remodeling.[8] Furthermore, the natural origin and known biocompatibility of alginate and MC, along with laponite-RDS at non-toxic concentrations, support the formulation's safety for tissue engineering. The consistent cell viability also suggests the stability of the hydrogel under physiological ionic conditions. Thus, despite the presence of charged polymers such as GelMA, MC, and alginate, no detrimental effects on cell viability were observed.

We next characterized fibrotic responses of the encapsulated keloid fibroblasts. Compared to normal dermal fibroblasts, patient-derived keloid fibroblasts showed significantly higher expression of ECM remodeling genes (*COL1*, *MMP2*, *LOX*), myofibroblast markers (ACTA2, Vimentin), the fibrosis-associated marker FSP1, and the inflammatory cytokine IL6 (Figure S3A and B). To assess the potential of the G*x*A*x*M*x*R*x* bioink for modeling fibrotic skin, we further examined gene expression responses to matrix stiffness. The stiffer G5A1M1R1 formulation induced markedly higher expression of *COL1* (~90%), *MMP2* (~70%), and *IL6* (~85%) compared to the softer G4A1M1R1 formulation (Figure 6B), demonstrating that even modest differences in stiffness can enhance the fibrotic and inflammatory phenotype of keloid fibroblasts in 3D culture. Additional upregulation of *FSP1* (~18%) and *LOX* (~20%) was also observed in G5A1M1R1, consistent with fibroblast activation and increased ECM crosslinking activity. These findings are consistent with prior reports that increased matrix stiffness promotes mechanosensitive signaling, fibroblast-to-myofibroblast differentiation, and excessive ECM remodeling, which are the hallmarks of fibrotic tissue pathology.[18,48,49]

To confirm these changes at the protein level, we performed immunofluorescence staining on single square-shaped 3D-printed constructs (adapted from a 3 × 3 grid pattern; Figure S2A). Positive expression of MTS1 (*FSP1*), F-actin, and α-SMA was observed in encapsulated keloid fibroblasts (Figure 6C–D), with substantially stronger signal intensity and greater cell aggregation in G5A1M1R1. These findings support the activation of myofibroblasts under stiff microenvironmental conditions. The transition of fibroblasts to myofibroblasts is a hallmark of skin fibrosis, characterized by elevated expression of α-SMA and FSP1, along with prominent actin stress fiber formation (F-actin).[50] Together, these findings suggest that the G*x*A*x*M*x*R*x* bioink provides a mechanically tunable and biocompatible platform for constructing simplified 3D models that recapitulate key features of fibrotic skin tissue. By integrating GelMA, alginate, MC, and laponite-RDS, we developed a structurally stable scaffold that supports cell viability and enables stiffness-dependent modulation of fibrotic gene expression. While preliminary, this system

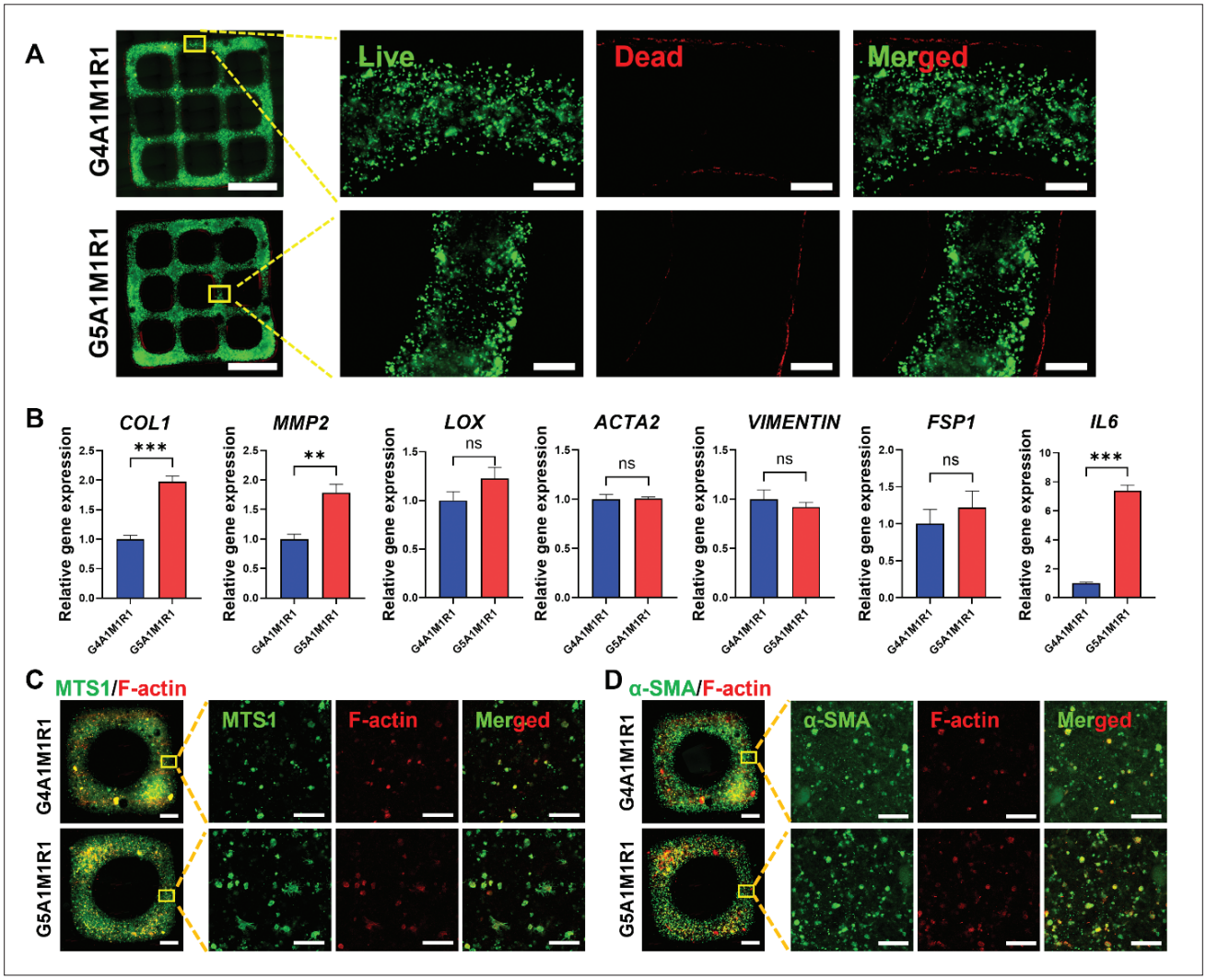

Figure 6. Fabrication of a keloid biomimetic disease model via encapsulation of keloid dermal fibroblasts in stiffness-controlled bioinks. (A) The biocompatibility of the hydrogel blend, comprising GelMA (4 and 5% w/v), alginate (1% w/v), MC (1% w/v), and laponite-RDS (1% w/v), is demonstrated by high cell viability, as indicated by Calcein-AM staining. Scale bars: 5 mm (magnified: 200×). (B) Keloid dermal fibroblasts remain functionally active when encapsulated in the hydrogel blend, maintaining their characteristic behavior. $n = 3$. $^{**}p < 0.01$, $^{***}p < 0.001$. (C, D) Pro-fibrotic response of keloid dermal fibroblasts was demonstrated by elevated expression of MTS1, α-SMA, and F-actin, as shown by immunofluorescence staining. Scale bars: 1 mm (magnified: 200×).

offers a foundational tool for future *in vitro* studies of keloid-associated fibroblast behavior. With further development, it may be adapted to include additional skin-resident cell types, such as keratinocytes, for the fabrication of more complex, multilayered tissue constructs.[51]

Although the current study focuses on the development and characterization of a mechanically tunable GelMA-based bioink for modeling fibrotic skin, the translational potential of this system could be further expanded through its drug delivery capability. GelMA hydrogels have been widely reported as promising platforms for localized and sustained drug release due to their tunable mesh size, physicochemical properties, and biocompatibility.[52,53] For instance, a GelMA-based drug delivery system has been shown to encapsulate albumin-bound paclitaxel (Abraxane®) with high efficiency (up to 96%) and achieve sustained release over several weeks by modulating GelMA concentration and enzymatic degradation kinetics, without compromising mechanical integrity.[54] Furthermore, systematic studies have demonstrated that drug loading, ionic strength, and environmental pH can significantly influence water states and hydrogel mesh size, thereby tuning drug retention and release behavior.[26] These findings suggest that the rheological and

crosslinking features of GelMA, well-preserved in our G*x*A*x*M*x*R*x* formulation, could support incorporation of antifibrotic therapeutics in future applications. Additionally, the high batch-to-batch reproducibility and controllability of GelMA production further enhance its clinical feasibility for biofabrication and drug screening platforms.[55] Therefore, while drug delivery was not directly addressed in this study, our bioink formulation may offer a dual-function system for stiffness-regulated disease modeling and therapeutic testing, warranting further investigation. Moreover, although degradation rates were evaluated and found to differ modestly across formulations (Figure S1C), other potentially influential parameters, including porosity and mesh size, which may impact both cellular responses and drug loading or release behavior, were not quantitatively characterized and should be systematically explored in future work.

Despite these promising results, several limitations should be acknowledged. First, the biological effects of individual bioink components, including alginate, MC, and laponite-RDS, were not independently assessed under stiffness-matched conditions, and thus compositional influences beyond mechanical cues cannot be fully excluded. Second, although the bioink formulation includes electrostatic interactions among charged polymers, its structural stability is primarily governed by GelMA photopolymerization. The impact of physiological ions or charged biomolecules, especially in the context of long-term culture or drug screening, remains to be investigated. Lastly, as this study focused on short-term fibrotic responses, future work should investigate long-term ECM remodeling, protein-level signaling pathways, and the incorporation of co-culture systems to more accurately model the complex pathophysiology of keloid disease. In particular, the current model is limited to fibroblast-only constructs, and future studies incorporating additional skin-resident cell types, such as keratinocytes, will be essential to more faithfully replicate the cellular heterogeneity and structural complexity of fibrotic skin tissue.

4. Conclusion

The 3D bioprinting has emerged as a transformative technology for fabricating complex, functional, and biomimetic tissue constructs by integrating living cells with tailored biomaterials and biochemical cues. In this study, we developed a composite bioink composed of GelMA, alginate, MC, and laponite-RDS, designed to achieve tunable mechanical properties, robust printability, and high biocompatibility. GelMA served as the primary crosslinkable backbone, forming stable networks upon UV exposure and providing cell-adhesive motifs essential for tissue integration. While alginate is conventionally used as an ionically crosslinked matrix, we leveraged it here as a viscoelasticity enhancer, demonstrating its utility even in the absence of calcium. The addition of MC improved mechanical resilience and contributed to the formation of a cohesive hydrogel network, while laponite-RDS, a nanoclay with high surface reactivity, significantly enhanced the rheological profile by boosting viscosity, shear-thinning behavior, and elastic modulus. This work establishes a mechanically tunable and cytocompatible bioink capable of supporting 3D bioprinting of keloid-like fibrotic tissue constructs. By maintaining constant bioink composition and modulating stiffness via GelMA concentration, we demonstrated that matrix mechanics alone can significantly influence the activation of patient-derived keloid fibroblasts. The platform holds promise for disease modeling and future applications in drug screening and regenerative medicine. While this study demonstrates proof-of-concept for stiffness-regulated fibrosis modeling, further work is needed to explore long-term culture responses, matrix remodeling, and the independent biological roles of individual hydrogel components under stiffness-matched conditions. Additionally, the impact of physiological ions or charged therapeutic molecules on bioink stability and drug-release behavior warrants investigation in future applications.

Acknowledgments

We thank the Soonchunhyang Biomedical Research Core-Facility of the Korea Basic Science Institute (KBSI) for providing access to essential instrumentation and technical support throughout this study.

Funding

This work was supported by the Soonchunhyang University Research Fund and the National Research Foundation of Korea funded by the Ministry of Science and ICT (MSIT) (grant numbers: RS-2019-NR040068, RS-2023-00284258, and 2017R1D1AB03029770).

Conflict of interest

The authors declare they have no competing interests.

Author contributions

Conceptualization: Laurensia Danis Anggradita, Seung Min Nam, Yongsung Hwang

Formal analysis: Laurensia Danis Anggradita, Sung Sik Hur, Taekyun Kim, Wonjong Seon,

Mohammed Aboobucker Sithique, Seung Min Nam, Yongsung Hwang

Funding acquisition: Seung Min Nam, Yongsung Hwang

Investigation: Laurensia Danis Anggradita, Seung Min Nam, Yongsung Hwang
Methodology: Laurensia Danis Anggradita, Seung Min Nam, Yongsung Hwang
Project administration: Seung Min Nam, Yongsung Hwang
Writing – original draft: Laurensia Danis Anggradita, Murugaiyan Manimohan, Sung Sik Hur,
Seung Min Nam, Yongsung Hwang
Writing – review & editing: Laurensia Danis Anggradita, Murugaiyan Manimohan,
Seung Min Nam, Yongsung Hwang
All authors have read and agreed to the published version of the manuscript.

Ethics approval and consent to participate

The study was conducted according to the guidelines of the Declaration of Helsinki and approved by the Institutional Review Board of Soonchunhyang University Bucheon Hospital (SCHBC_IRB_2017-08-010). Informed consent was obtained from all individual participants included in the study.

Consent for publication

Not applicable.

Availability of data

The data that support the findings of this study are available from the corresponding author upon reasonable request.

References

1. Gu BK, Choi DJ, Park SJ, Kim MS, Kang CM, Kim C-H. 3-Dimensional bioprinting for tissue engineering applications. *Biomater Res*. 2016;20(1):12. doi: 10.1186/s40824-016-0058-2
2. Choi K, Park CY, Choi JS, *et al*. The effect of the mechanical properties of the 3D printed gelatin/hyaluronic acid scaffolds on hMSCs differentiation towards chondrogenesis. *Tissue Eng Regen Med*. 2023;20(4):593-605. doi: 10.1007/s13770-023-00545-w
3. Rossi A, Pescara T, Gambelli AM, *et al*. Biomaterials for extrusion-based bioprinting and biomedical applications. *Front Bioeng Biotechnol*. 2024;12:1393641. doi: 10.3389/fbioe.2024.1393641
4. Chen XB, Fazel Anvari-Yazdi A, Duan X, *et al*. Biomaterials/bioinks and extrusion bioprinting. *Bioact Mater*. 2023;28:511-536. doi: 10.1016/j.bioactmat.2023.06.006
5. Yoon J, Han H, Jang J. Nanomaterials-incorporated hydrogels for 3D bioprinting technology. *Nano Converg*. 2023;10(1):52. doi: 10.1186/s40580-023-00402-5
6. Nath R, Thomas J, Janardanan A, *et al*. An insight into synthesis, properties and applications of gelatin methacryloyl hydrogel for 3D bioprinting. *Mater Adv*. 2023;22:5496-5529. doi: 10.1039/D3MA00715D
7. Wu Y, Xiang Y, Fang J, *et al*. The influence of the stiffness of GelMA substrate on the outgrowth of PC12 cells. *Biosci Rep*. 2019;39(1):BSR20181748. doi: 10.1042/BSR20181748
8. Piao Y, You H, Xu T, *et al*. Biomedical applications of gelatin methacryloyl hydrogels. *Eng Regen*. 2021;2:47-56. doi: 10.1016/j.engreg.2021.03.002
9. Axpe E, Oyen ML. Applications of alginate-based bioinks in 3D bioprinting. *Int J Mol Sci*. 2016;17(12):1976. doi: 10.3390/ijms17121976
10. Aldana AA, Valente F, Dilley R, Doyle B. Development of 3D bioprinted GelMA-alginate hydrogels with tunable mechanical properties. *Bioprinting*. 2021;21:e00105. doi: 10.1016/j.bprint.2020.e00105
11. Contessi N, Altomare L, Filipponi A, Farè S. Thermo-responsive properties of methylcellulose hydrogels for cell sheet engineering. *Mater Lett*. 2017;207:157-160. doi: 10.1016/j.matlet.2017.07.023
12. Chang C, Zhang L. Cellulose-based hydrogels: present status and application prospects. *Carbohydr Polym*. 2011;84(1):40-53. doi: 10.1016/j.carbpol.2010.12.023
13. Contessi Negrini N, Bonetti L, Contili L, Farè S. 3D printing of methylcellulose-based hydrogels. *Bioprinting*. 2018;10:e00024. doi: 10.1016/j.bprint.2018.e00024
14. Ma Z, He H, Deng C, *et al*. 3D bioprinting of proangiogenic constructs with induced immunomodulatory microenvironments through a dual cross-linking procedure using laponite incorporated bioink. *Compos B Eng*. 2022;229:109399. doi: 10.1016/j.compositesb.2021.109399
15. Choi D, Heo J, Aviles Milan J, *et al*. Structured nanofilms comprising Laponite® and bone extracellular matrix for osteogenic differentiation of skeletal progenitor cells. *Mater Sci Eng C Mater Biol Appl*. 2021;118:111440. doi: 10.1016/j.msec.2020.111440
16. Li C, Hou Y, He M, *et al*. Laponite lights calcium flickers by reprogramming lysosomes to steer DC migration for an effective antiviral CD8(+) T-cell response. *Adv Sci (Weinh)*. 2023;10(30):e230300. doi: 10.1002/advs.202303006.
17. Wang Y, Zhao T, Jiao Y, *et al*. Silicate nanoplatelets promotes neuronal differentiation of neural stem cells and restoration of spinal cord injury. *Adv Healthc Mater*. 2023;12(19):e2203051. doi: 10.1002/adhm.202203051.

18. Kim H, Anggradita LD, Lee SJ, *et al*. Ameliorating fibrotic phenotypes of keloid dermal fibroblasts through an epidermal growth factor-mediated extracellular matrix remodeling. *Int J Mol Sci*. 2021;22(4):2198. doi: 10.3390/ijms22042198

19. Olejnik A, Semba JA, Kulpa A, Dańczak-Pazdrowska A, Rybka JD, Gornowicz-Porowska J. 3D bioprinting in skin related research: recent achievements and application perspectives. *ACS Synth Biol*. 2022;11(1):26-38. doi: 10.1021/acssynbio.1c00547

20. Kwon SH, Lee J, Yoo JA-O, Jung YA-O. Artificial keloid skin models: understanding the pathophysiological mechanisms and application in therapeutic studies. *Biomater Sci*. 2024;25(13):3321-3334. doi: 10.1039/d4bm00005

21. Kang H, Shih Y-RV, Hwang Y, *et al*. Mineralized gelatin methacrylate-based matrices induce osteogenic differentiation of human induced pluripotent stem cells. *Acta Biomater*. 2014;10(12):4961-4970. doi: 10.1016/j.actbio.2014.08.010.

22. Temirel M, Dabbagh SR, Tasoglu S. Shape fidelity evaluation of alginate-based hydrogels through extrusion-based bioprinting. *J Funct Biomater*. 2022;13(4):225. doi: 10.3390/jfb13040225

23. Livak KJ, Schmittgen TD. Analysis of relative gene expression data using real-time quantitative PCR and the 2(-Delta Delta C(T)) method. *Methods*. 2001;25(4):402-8. doi: 10.1006/meth.2001.1262. PMID: 11846609.

24. Wang K-Y, Jin X-Y, Ma Y-H, *et al*. Injectable stress relaxation gelatin-based hydrogels with positive surface charge for adsorption of aggrecan and facile cartilage tissue regeneration. *J Nanobiotechnol*. 2021;19(1):214. doi: 10.1186/s12951-021-00950-0

25. Vigata M, Meinert C, Bock N, Dargaville BL, Hutmacher DW. Deciphering the molecular mechanism of water interaction with gelatin methacryloyl hydrogels: role of ionic strength, pH, drug loading and hydrogel network characteristics. *Biomedicines*. 2021;9(5):574. doi: 10.3390/biomedicines9050574

26. Xiao S, Zhao T, Wang J, *et al*. Gelatin methacrylate (GelMA)-based hydrogels for cell transplantation: an effective strategy for tissue engineering. *Stem Cell Rev Rep*. 2019;15(5):664-679. doi: 10.1007/s12015-019-09893-4.

27. Fang W, Yang M, Wang L, *et al*. Hydrogels for 3D bioprinting in tissue engineering and regenerative medicine: current progress and challenges. *Int J Bioprint*. 2023;9(5):759. doi: 10.18063/ijb.759. PMID: 37457925

28. Stealey ST, Gaharwar AK, Zustiak SP. Laponite-based nanocomposite hydrogels for drug delivery applications. *Pharmaceuticals*. 2023;16(6):821. doi: 10.3390/ph16060821

29. de Barros NR, Gomez A, Ermis M, *et al*. Gelatin methacryloyl and Laponite bioink for 3D bioprinted organotypic tumor modeling. *Biofabrication*. 2023;15(4):045005. doi: 10.1088/1758-5090/ace0db

30. Ashammakhi N, Ahadian S, Xu C, *et al*. Bioinks and bioprinting technologies to make heterogeneous and biomimetic tissue constructs. *Mater Today Bio*. 2019;1:100008. doi: 10.1016/j.mtbio.2019.100008

31. Muthuramalingam K, Lee HA-O. Effect of GelMA hydrogel properties on long-term encapsulation and myogenic differentiation of C(2)C(12) spheroids. *Gels*. 2023;9(12):925. doi: 10.3390/gels9120925.

32. Gao T, Gillispie GJ, Copus JS, *et al*. Optimization of gelatin-alginate composite bioink printability using rheological parameters: a systematic approach. *Biofabrication*. 2018;10(3):034106. doi: 10.1088/1758-5090/aacdc7.

33. Moreira R, Chenlo F, Silva C, Torres MD. Rheological behaviour of aqueous methylcellulose systems: effect of concentration, temperature and presence of tragacanth. *LWT*. 2017;84:764-770. doi: 10.1016/j.lwt.2017.06.050

34. Schütz K, Placht A-M, Paul B, Brüggemeier S, Gelinsky M, Lode A. Three-dimensional plotting of a cell-laden alginate/methylcellulose blend: towards biofabrication of tissue engineering constructs with clinically relevant dimensions. *J Tissue Eng Regen Med*. 2017;11(5):1574-1587. doi: 10.1002/term.2058

35. Rastin H, Ormsby RT, Atkins GJ, Losic DA-OX. 3D bioprinting of methylcellulose/gelatin-methacryloyl (MC/GelMA) bioink with high shape integrity. *ACS Appl Bio Mater*. 2020;3(3):1815-1826. doi: 10.1021/acsabm.0c00169

36. Afghah F, Altunbek M, Dikyol C, Koc B. Preparation and characterization of nanoclay-hydrogel composite support-bath for bioprinting of complex structures. *Sci Rep*. 2020;10(1):5257. doi: 10.1038/s41598-020-61606-x

37. Mignon A, Pezzoli D, Prouvé E, *et al*. Combined effect of laponite and polymer molecular weight on the cell-interactive properties of synthetic PEO-based hydrogels. *React Funct Polym*. 2019;136:95-106. doi: 10.1016/j.reactfunctpolym.2018.12.017

38. Aazmi A, Zhang D, Mazzaglia C, *et al*. Biofabrication methods for reconstructing extracellular matrix mimetics. *Bioact Mater*. 2023;31:475-496. doi: 10.1016/j.bioactmat.2023.08.018.

39. GhavamiNejad A, Ashammakhi N, Wu XY, Khademhosseini A. Crosslinking strategies for 3D bioprinting of polymeric hydrogels. *Small*. 2020;16(35):2002931. doi: 10.1002/smll.202002931

40. Karaca MA, Khalili V, Ege D. Highly flexible methyl cellulose/gelatin hydrogels for potential cartilage tissue engineering applications. *Biopolymers*. 2025;116(1):e23641. doi: 10.1002/bip.23641

41. Šebenik U, Lapasin R, Krajnc M. Rheology of aqueous dispersions of laponite and TEMPO-oxidized nanofibrillated cellulose. *Carbohydr Polym*. 2020;240:116330. doi: 10.1016/j.carbpol.2020.116330

42. Yue K, Trujillo-de Santiago G, Alvarez MM, Tamayol A, Annabi N, Khademhosseini A. Synthesis, properties, and biomedical applications of gelatin methacryloyl (GelMA) hydrogels. *Biomaterials*. 2015;73:254-271. doi: 10.1016/j.biomaterials.2015.08.045

43. Li H, Chen S, Dissanayaka WL, Wang M. Gelatin methacryloyl/sodium alginate/cellulose nanocrystal inks and 3D printing for dental tissue engineering applications. *ACS Omega*. 2024;9(49):48361-48373. doi: 10.1021/acsomega.4c06458

44. Xu L, Zhang Z, Jorgensen AM, *et al*. Bioprinting a skin patch with dual-crosslinked gelatin (GelMA) and silk fibroin (SilMA): an approach to accelerating cutaneous wound healing. *Mater Today Bio*. 2023;18:100550. doi: 10.1016/j.mtbio.2023.100550

45. Zeimaran E, Pourshahrestani S, Röder J, Detsch R, Boccaccini AR. 3D printing of photocrosslinked alginate dialdehyde-gelatin hydrogels reinforced with cobalt-containing mesoporous bioactive glass nanoparticles for developing skin wound dressings. *Adv Mater Interfaces*. 2025;12(11):2400913. doi: 10.1002/admi.202400913

46. Limandjaja GC, Niessen FB, Scheper RJ, Gibbs S. The Keloid disorder: heterogeneity, histopathology, mechanisms and models. *Front Cell Dev Biol*. 2020;8:360. doi: 10.3389/fcell.2020.00360.

47. Hsu CK, Lin HH, Harn HI, *et al*. Caveolin-1 controls hyperresponsiveness to mechanical stimuli and fibrogenesis-associated RUNX2 activation in keloid fibroblasts. *J Invest Dermatol*. 2018;138(1):208-218. doi: 10.1016/j.jid.2017.05.041

48. Saraswati S, Marrow SMW, Watch LA, Young PP. Identification of a pro-angiogenic functional role for FSP1-positive fibroblast subtype in wound healing. *Nat Commun*. 2019;10(1):3027. doi: 10.1038/s41467-019-10965-9

49. Camman M, Nieswic N, Joanne P, *et al*. Fibrotic-like collagen matrices as innovative 3D in vitro models for investigating the impact of pathological ECM on muscle regeneration in muscular dystrophies. *bioRxiv*. 2024. doi: 10.1101/2024.12.23.630059

50. Tai Y, Woods EL, Dally J, *et al*. Myofibroblasts: function, formation, and scope of molecular therapies for skin fibrosis. *Biomolecules*. 2021;11(8):1095. doi: 10.3390/biom11081095

51. Lee W, Debasitis JC, Lee VK, *et al*. Multi-layered culture of human skin fibroblasts and keratinocytes through three-dimensional freeform fabrication. *Biomaterials*. 2009;30(8):1587-1595. doi: 10.1016/j.biomaterials.2008.12.009

52. Jang Y, Jang J, Kim BY, Song YS, Lee DY. Effect of gelatin content on degradation behavior of PLLA/gelatin hybrid membranes. *Tissue Eng Regen Med*. 2024;21(4):557-569. doi: 10.1007/s13770-024-00626-4

53. Lee YJ, Oh JH, Park S, *et al*. The application of L-serine-incorporated gelatin sponge into the calvarial defect of the ovariectomized rats. *Tissue Eng Regen Med*. 2025;22(1):91-104. doi: 10.1007/s13770-024-00686-6

54. Vigata M, Meinert C, Pahoff S, Bock N, Hutmacher DW. Gelatin methacryloyl hydrogels control the localized delivery of albumin-bound paclitaxel. *Polymers*. 2020;12(2):501. doi: 10.3390/polym12020501

55. Zhu M, Wang Y, Ferracci G, Zheng J, Cho NJ, Lee BH. Gelatin methacryloyl and its hydrogels with an exceptional degree of controllability and batch-to-batch consistency. *Sci Rep*. 2019;9(1):6863. doi: 10.1038/s41598-019-42186-x